Structure
Article

Crystal and Solution Structures of a Prokaryotic M16B Peptidase: an Open and Shut Case

Alexander E. Aleshin,[1] Svetlana Gramatikova,[1] Gregory L. Hura,[2] Andrey Bobkov,[1] Alex Y. Strongin,[1] Boguslaw Stec,[1] John A. Tainer,[3,4] Robert C. Liddington,[1,*] and Jeffrey W. Smith[1,*]
[1]Burnham Institute for Medical Research, 10901 North Torrey Pines Rd., La Jolla, CA 92037, USA
[2]Physical Bioscience Division
[3]Life Science Division
Lawrence Berkeley National Laboratory, Berkeley, CA 94720, USA
[4]Present address: Department of Molecular Biology and The Skaggs Institute for Chemical Biology, The Scripps Research Institute, La Jolla, CA, USA.
*Correspondence: rlidding@burnham.org (R.C.L.), jsmith@burnham.org (J.W.S.)
DOI 10.1016/j.str.2009.09.009

SUMMARY

The M16 family of zinc peptidases comprises a pair of homologous domains that form two halves of a "clam-shell" surrounding the active site. The M16A and M16C subfamilies form one class ("peptidasomes"): they degrade 30–70 residue peptides, and adopt both open and closed conformations. The eukaryotic M16B subfamily forms a second class ("processing proteases"): they adopt a single partly-open conformation that enables them to cleave signal sequences from larger proteins. Here, we report the solution and crystal structures of a prokaryotic M16B peptidase, and demonstrate that it has features of both classes: thus, it forms stable "open" homodimers in solution that resemble the processing proteases; but the clam-shell closes upon binding substrate, a feature of the M16A/C peptidasomes. Moreover, clam-shell closure is required for proteolytic activity. We predict that other prokaryotic M16B family members will form dimeric peptidasomes, and propose a model for the evolution of the M16 family.

INTRODUCTION

Metalloendopeptidases of the M16 family form a unique family that is distinct from conventional peptidases. They recognize substrates by encapsulating them inside a catalytic chamber (Malito et al., 2008), and recognize targets with nonhomologous sequences (Shen et al., 2006; Taylor et al., 2001). M16 peptidases are present in most prokaryotic and eukaryotic organisms, but specific cellular functions have been assigned in only a few cases (Bhushan et al., 2003; Deng et al., 2001; Eggleson et al., 1999; Kurochkin, 2001; Taylor et al., 2001). Some eukaryotic members have been linked to chronic and degenerative diseases, including diabetes and Alzheimer's (Cabrol et al., 2009; Farris et al., 2003; Kwak et al., 2008; Selkoe, 2001; Sun and Alkon, 2006), which has raised interest in the entire M16 family and highlighted the need for broader insights into structure-function relationships that would expedite the assignment of cellular function.

All M16 peptidases possess an inverted zinc-binding motif (HxxEH) (Becker and Roth, 1992; Rawlings and Barrett, 1991) at their active sites, a rare feature shared only with peptidases from the poxvirus family, M44 (Hedengren-Olcott et al., 2004). They have been divided into three subfamilies (A–C), based on sequence alignments and subunit connectivity (Figure 1A). The A and C subfamilies have similar organizations and activities, and are here considered as a single functional class: thus, in both cases, catalytic activity resides in a single polypeptide chain of ~1000 residues, comprising a tandem pair of ~500-residue domains (connected by a long linker) with low sequence homology but very similar structures. The N-terminal domain contains the zinc-binding motif, but the C-terminal domain is also required for activity (Johnson et al., 2006; Li et al., 2006). They degrade a variety of polypeptides and folded subdomains 30-70 residues long (such as the β-chain of insulin), and are here referred to as "peptidasomes" (Johnson et al., 2006), based on their structural and functional resemblance to proteasomes.

In the case of eukaryotic M16B proteases, the two ~500-residue domains are encoded by separate genes, and form functional heterodimers. Their tertiary structures are very similar to each other and to the M16A/C class, and only one domain contains the zinc-binding motif. However, they have a related but distinct function. M16B peptidases do not degrade folded subdomains; instead, they cleave off the short targeting sequences at the N termini of proteins transported to mitochondria and chloroplasts. For this reason, they are called "processing peptidases" (Deng et al., 2001; Taylor et al., 2001), and are here considered as a distinct functional class.

All M16 family members have a similar organization in which each domain forms one half of a clam-shell, which has been observed in closed, open, and locked-open states. The M16A protein, insulin-degrading enzyme (IDE) (Shen et al., 2006), crystallized as a closed clam-shell with substrate locked inside its central chamber, whereas another M16A protein, *E. coli* pitrilysin (Protein Data Bank [PDB] entry 1Q2L), crystallized in an open conformation in the absence of peptide. The crystal structure of one M16C protein, *A. thaliana* PreP (Johnson et al., 2006), has been determined in the presence of substrate, and it forms a closed clam-shell very similar to that of IDE. In both cases,

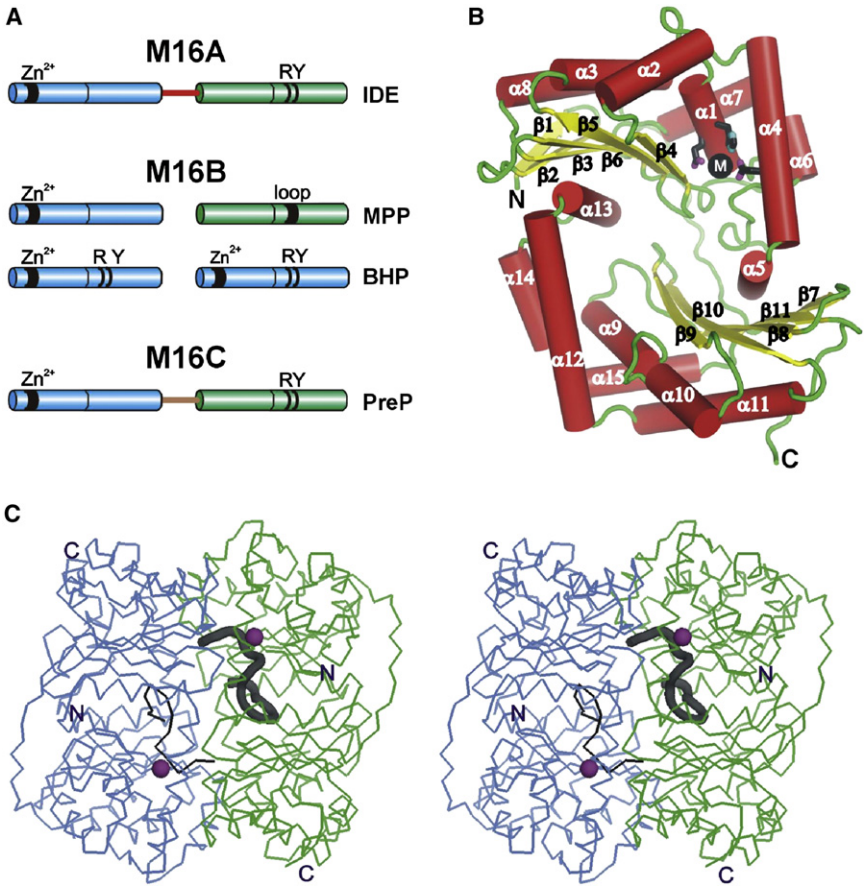

Figure 1. Structural Organization of BHP

(A) Domain organization of the M16 peptidases. The key features are: the inverted Zn^{2+}-binding motif (HXXEH), the "peptidasome" motif (R,Y), and the "processing peptidase" motif (the long glycine-rich loop).

(B) The BHP monomer viewed down the pseudo-dyad relating the two subdomains, showing the two β sheets (in yellow), the metal ion ("M") associated with the N-terminal subdomain, and the two α-helical bundles in red, which pack head-to-tail. The core β sheet topology (2-6-3-5-4) is different from that in thermolysin, causing the Zn-binding helix (α1) to run in the opposite direction, hence the inversion of the zinc-binding motif. The N-terminal subdomain has an extra β strand (β1) at its N terminus and an extra helix (α8) at its C terminus. The subdomains are connected by a linker running close to the local dyad.

(C) Stereo view of the BHP homodimer viewed down the molecular dyad. The monomers are in green and blue. The bound peptide, and its symmetry-related counterpart, are shown as thick and thin ribbons. The two active-site metal ions are in magenta.

a single active site is located within the clamshell at the interface between the two domains. These observations have led to a model in which the binding of peptide to the open conformation promotes closure of the clamshell and activation of the enzyme (Johnson et al., 2006; Shen et al., 2006). However, Im et al. (Im et al., 2007) have proposed a more sophisticated model for IDE in which the enzyme adopts a default closed conformation, implying a further level of regulation, because the clam-shell must open to allow access of substrate.

Two crystal structures of eukaryotic M16B proteins have been determined: the mitochondrial processing peptidase (MPP) (Taylor et al., 2001) and the cytochrome BC1 complex (BC1) (Xia et al., 1997). These enzymes crystallized in a partly open conformation both in the presence or absence of substrate. Their structures also revealed a novel structural element called the "glycine-rich loop," which prevented complete closure of the clamshell (Nagao et al., 2000; Taylor et al., 2001). A partially open, locked conformation is consistent with the function of this class of enzymes: selectively cleaving the unstructured N-terminal tails of folded protein domains that are too large to fit into the active site.

Bioinformatics analysis has pointed to the existence of prokaryotic members of the M16B subfamily, although their biological functions are unknown. The MEROPS database (Rawlings et al., 2008) subdivides them further into four groups: M16B.014, M16B.016, M16B.UPB, and M16B.UNB, each comprising a single ~500 residue domain (although a few M16B.UPB members have the two domains fused, analogous to the M16A/C class). Except for the M16B.UNB group, these prokaryotic proteins possess a zinc-binding motif, and all have reasonable homology (up to 30% identity) with their eukaryotic M16 counterparts. It was therefore initially assumed that their activities would be related (Bolhuis et al., 2000; Kitada et al., 2007), although it should be noted that they do not contain the long glycine-rich loop insertions characteristic of the eukaryotic M16B enzymes. Recent reports have suggested further intriguing differences. Thus, M16B.016 enzymes from *Bacillus halodurans* and *Rickettsia prowazekii* have proteolytic activity as single gene products, cleaving oligopeptide substrates in vitro (Dabonne et al., 2005; Kitada et al., 2007; Ohtsuka et al., 2009); indeed, the authors proposed that the M16B.016 enzymes are monomeric, which would suggest a distinct catalytic mechanism.

In order to provide definitive data on the organization and function of the prokaryotic M16B proteases, we determined the crystal structure of the BH2405 gene product of *Bacillus halodurans* C-125 strain (referred to here as BHP), which is classified in the M16B.016 group. In contrast to previous reports, we found that BHP forms stable dimers both in solution and in the crystal. We provide evidence that the open dimer resembles its eukaryotic M16B orthologs, but that substrate binding induces complete domain closure to a state that closely resembles the M16A/C class, consistent with its biochemical activity in which it functions as a peptidasome rather than a processing protease. We further provide direct evidence that domain closure is required for catalytic activity. Finally, the "hybrid" characteristics of BHP place it in a distinct category that provides novel insights into the evolution of the entire M16 family.

RESULTS AND DISCUSSION

BHP Is a Dimer in Solution

A previous report on an almost identical peptidase from a different strain of *B. halodurans* (99% identity, called here "BH4") suggested that the active species was monomeric (Dabonne et al., 2005). By gel filtration, BHP eluted as a single peak with an apparent molecular weight (MW) of 69 kDa, intermediate between a monomer and dimer (calculated MWs are 47.5 and 95 kDa) (see Figures S1A and S1B available online). We therefore used analytical ultracentrifugation (AUC), which provides an accurate, shape-independent determination of MW in solution. Equilibrium sedimentation experiments by AUC demonstrated unequivocally that BHP forms a dimer in solution at physiological salt concentrations, with a $K_d \leq 20$ nM (Figure S1C), and that an inactive mutant preincubated with insulin-B had a similar K_d. It is therefore very likely that BH4 also functions as a dimer.

Crystal Structure of BHP

The crystal structure was solved by molecular replacement and refined to a resolution of 2.75 Å (Table 1). Crystals grew in the presence of a molar excess of Co^{2+} ions, an inhibitor of the enzyme (Dabonne et al., 2005). EXAFS scans of crystals demonstrated the presence of Co^{2+} and the complete absence of Zn^{2+} ions. In the crystals, each active site is occupied by a single metal ion (as judged by anomalous difference Fourier maps), which we therefore assume to be Co^{2+}.

BHP forms a homodimer in the crystals with a closed clam-shell architecture (Figure 1C) similar to those of the M16A/C peptidasomes, IDE and PreP. The two halves of the BHP dimer are very similar, with a root-mean-square deviation (rmsd) of 0.38 Å for 408 superposed Cα atoms. When compared with the other known structures of M16 proteases, the BHP monomer overlays with a typical rmsd of ~1.5 Å for ~70% of their Cα atoms. The interface between the BHP monomers involves multiple interactions involving ~73 residues (out of 414) from each monomer, burying a large surface area (~2700 Å^2), which is comparable in size with the closed clamshells of IDE and PreP. The interface creates a closed water-filled chamber with a volume of ~10,000 Å^3, similar to PreP, but smaller than in IDE (Malito et al., 2008). Because there are no channels through which a peptide could enter, the clam-shell must open at least transiently in order to bind substrate.

Each monomer of BHP consists of two structurally similar subdomains (residues 1–207 and 223–415) connected by a long linker and related by an approximate 2-fold axis of symmetry (although only the N-terminal subdomain contains the Zn^{2+}-binding motif) (Figures 1B, 2). Each subdomain has a core with a 3-dimensional structure reminiscent of thermolysin, but with a different topology (Makarova and Grishin, 1999), comprising a 5-stranded antiparallel β sheet and a helical bundle that packs against the convex face of the sheet. As in thermolysin, the active site is formed by the packing of the α helix (α1 in this case) containing the Zn-binding motif against one edge of the sheet; however, there are also critical contributions from the second monomer (see below). The two subdomains pack head-to-tail, by inserting a quasi-equivalent helix into the concave face of the "other" β sheet. This arrangement creates one half of the catalytic cavity, and is sealed at the top by the packing of β5-β6 loops and the inter-subdomain linker.

Table 1. Data Collection and Refinement Statistics

Space Group	$C222_1$
Unit cell/Å	$a = 91.1, b = 194.0, c = 125.6$
Resolution/Å (outer shell)	2.75 (2.75-3.0)
Unique reflections collected	27312
$<I/\sigma(I)>$	20 (1.9)
Completeness (%)	94 (75)
Average redundancy	6.5 (3.6)
R_{merge}	0.092 (0.54)
Refinement statistics	
R_{work} (R_{free})	0.198 (0.268)
Rmsd	
Bond lengths (Å)	0.007
Bond angles (Å)	1.23
Ramachandran plot (%)	
Most preferred	87
Allowed	12
Generously allowed	1
Disallowed	0
Number of protein residues	2 × 414
Ligands and solvent	
Substrate residues	2 × 17
Other ligands	2 Co^{2+}, 6 SO_4^{2-}
Water molecules	260
Temperature factors (Å^2)	
Protein average	59
Co^{2+}	45
Peptide	90
Wilson B	66

Peptide Binding and Substrate Specificity

Because BHP is a homodimer, it has two active sites. Both sites contain a continuous stretch of electron density consistent with a bound peptide ligand (Figure 3A). Because we did not add peptide at any point, the bound ligand was either copurified with BHP or generated by autolytic digestion during the crystallization process. The relatively weak electron density suggests an occupancy of ~50%. However, it is also possible that each BHP dimer binds a single peptide at full occupancy, but that given a stochastic distribution of peptides between the two crystallographically distinct sites, only an averaged image with partial occupancy is observed.

The electron density was not of sufficient clarity to resolve the peptide sequence(s). Nevertheless, phase refinement utilizing the noncrystallographic dyad allowed us to model the ligand as a polyalanine chain with a length of ~17 residues (Figure 1C). Superposition of BHP with IDE bound to the amylin peptide (PDB entry 2G48) shows that both substrates have similar conformations near the active sites (Figure 3B). In both cases, the N and the C termini of the peptides interact with apposing halves of the clam-shell, stabilizing the closed conformation.

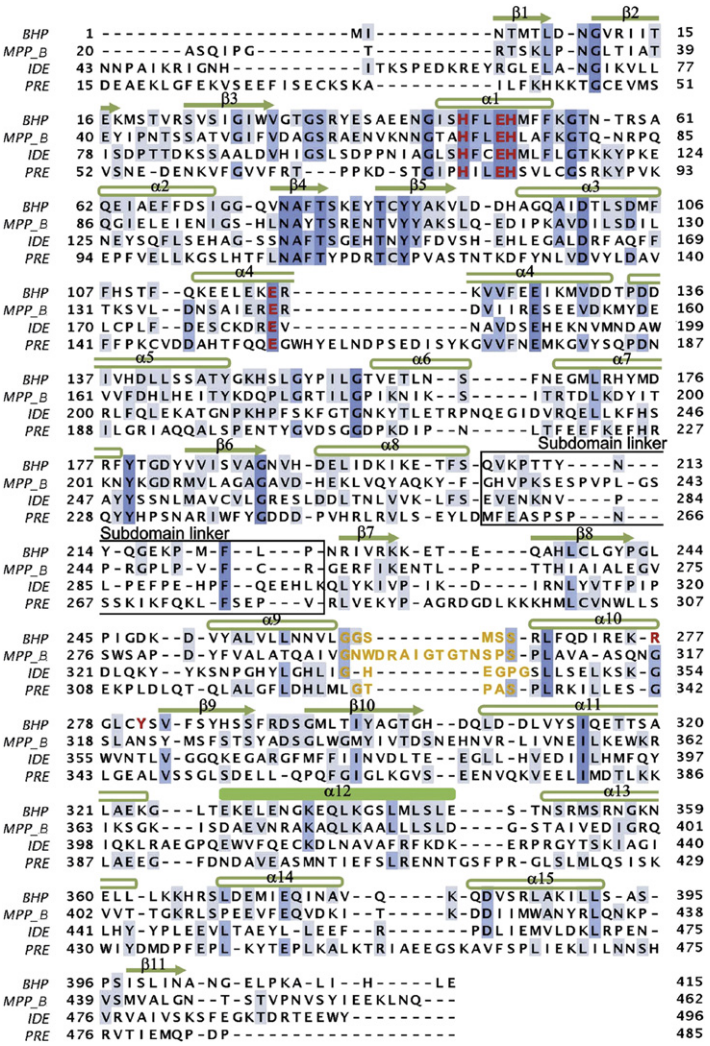

Figure 2. Primary Sequence Alignments and Secondary Structure Assignments for BHP

The sequence is aligned with the Zn-binding subunits of βMPP, IDE, and PreP (UniProt accession numbers P10507, P14735, and Q9LJL3, respectively). Strands and helices are numbered as in Ohtsuka et al. (2009). Blue shading indicates degree of conservation. Active-site residues are in red; glycine-rich loops in yellow. The "hinge" helix (α12) in BHP is marked in solid green, and the subdomain linker is boxed. Alignments with the "noncatalytic" subunits of the same proteins are shown in Figure S2.

A previous analysis of the cleavage specificity of the close ortholog, BH4, revealed a preference for aromatic residues at P1 (upstream of the cleavage site), and a broader preference at P1′ (downstream of the cleavage site), including hydrophobic/aromatic residues and arginine (Dabonne et al., 2005). The structure of BHP is consistent with these preferences. Thus, the S1 site is flat, and its preference for aromatic residues may arise from favorable stacking interactions with F78 from the β4 strand, which is conserved in M16 peptidasomes (Figure 2). The S1′ site is a deep pocket (Figure 4B) with hydrophobic walls and acidic residues at the base. The hydrophobic lining presumably favors hydrophobic residues, whereas the side chain of arginine is long enough to extend to the base of the pocket and interact with the acidic groups.

The electrostatic potential and shape of other M16 proteases near to the active sites are similar, suggesting a similar cleavage specificity. However, there is evidence that in many cases M16 substrate recognition is more complex. For example, IDE activity is sensitive to point mutations in its substrate far from the cleavage sites, which occurs at discrete positions but with limited consensus at the P1 and P1′ positions (Malito et al., 2008; Shen et al., 2006; Taylor et al., 2001). Beyond the immediate environment of the active site, the charge distribution and shape of the peptidasome chambers are highly variable (Figure 4A), so that conclusions about sequence specificity drawn from the cleavage of short peptides may not translate into substrate specificity in vivo.

Clam-Shell Closure Enhances Catalytic Activity

Helix α1, which harbors the Zn^{2+}-binding motif, ^{46}HxxEH^{50}, packs against one end of the convex surface of its β sheet. H46 and H50 coordinate the metal directly, E49 acts as a general base in the cleavage reaction, and E126 from helix α4 completes the coordination site. The active site is completed by elements from the C-terminal portion of the second monomer (Figures 3 and 4B). In particular, Y281, which lies within 4.5 Å of the metal ion, as well as the neighboring R274, are well-positioned to bind the main-chain carbonyl oxygens of the substrate at positions P1′ and P2′. The conservation and importance of a similar R/Y pair in the M16A/C peptidasomes was previously noted for PreP (Johnson et al., 2006); for IDE (Shen et al., 2006), however, a Y→ F mutation had a minor effect, but a Y→ A mutation abrogated activity. We generated a Y281F mutant in BHP to explore its role in catalysis, and found that its activity (as judged by its initial velocity measured at 0.5 μM enzyme, 10 μM fluorogenic peptide [substrate-V]) was undetectable (at least 2000-fold less than wild-type) (Figure 4C). This effect was greater than for the active site mutant, E49Q, which had a measurable but low activity (initial velocity reduced 200-fold).

BHP is a functional homodimer with two symmetry-related active sites, providing an unusual opportunity to define the precise role of clam-shell closure in the activity of BHP, and perhaps peptidasomes in general. When the two mutant dimers, E49Q and Y281F, are incubated together, interchange of monomers between dimers creates a subpopulation of heterodimers that have one active site doubly mutated (E49Q/Y281F) while the other is wild-type, i.e., self-complementation. When the two mutants were incubated for 10 min at 25°C, we did indeed observe a significant increase in enzymatic activity compared with either single mutant (Figure 4C). This experiment provides convincing evidence that domain closure promotes or is required for catalytic activity. Presumably, a higher degree of complementation was not achieved for a related reason – that the Y→ F change at the second site destabilized the closed clam-shell conformation to a significant extent. The observation that peptidasomes are unable to cleave peptides that do not fit into

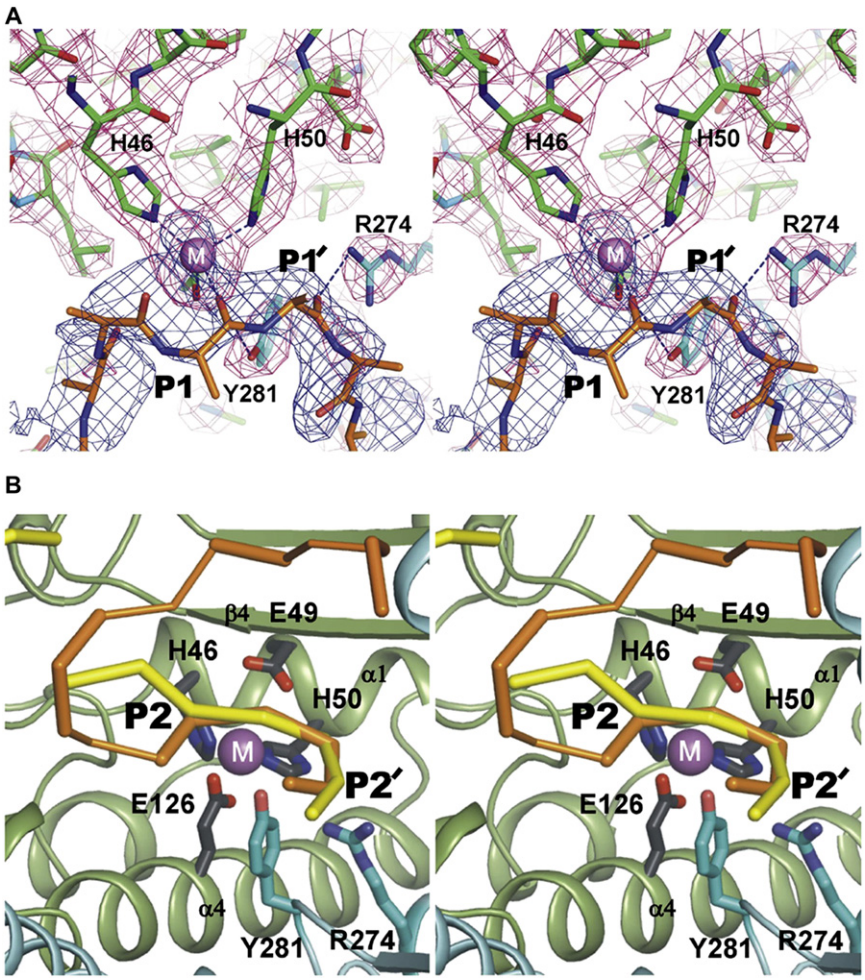

Figure 3. The Active Site of BHP

(A) Stereo view of the electron density map around the active site. The two monomers contributing to the active site are in green and blue; the substrate is built as a polyalanine chain in orange/red/blue. The cobalt ion is labeled "M." A 2Fo-Fc map covering the protein is contoured at 2σ and colored red. The peptide map (blue) is an averaged Fo-Fc map contoured at 2.5σ.

(B) A broader view of the active site, with selected side-chains shown, including Y281 and R274 (in cyan) from the second monomer. The peptide model (orange; the thinner lines indicate weak or discontinuous density) is compared with the peptide (yellow) observed in IDE (PDB entry 2G48) after overlaying the protein models. The P2-P2′ segments (Cα positions) of the two peptides overlay well, but deviate thereafter.

the closed catalytic chamber (Johnson et al., 2006; Shen et al., 2006) is one obvious corollary of this model.

Modeling an Open Dimer Conformation for BHP

The tight binding between BHP monomers ($K_d \leq 20$ nM) indicates that it is predominantly a homodimer both in the presence and absence of substrate. Because the dimer must open to allow substrate entry and product release, we sought to model the open conformation. When comparing BHP with the eukaryotic M16B proteases (which are locked in a partly open conformation), we noted a striking similarity between the quaternary organization at the "open" interface and the same region of the closed interface of BHP (Figures 5, S3, and S4). The interface buries ~1800 Å^2 in MMP and BC1, which is less than that of the closed conformation of BHP (~2700 Å^2), but sufficient to form stable dimers in solution. Indeed, individual monomers of BHP overlay well onto the two half clam-shells of either MPP or BC1, and the conformational differences between them can be approximated as a rigid body rotation about an axis passing close to the long axes of helix α12 and its symmetry mate across the dimer axis (but see below).

An opening mechanism that maintains an extensive interface is critical for BHP, because it comprises two polypeptide chains that must remain paired throughout the catalytic cycle. By contrast, the M16A/C domains are connected covalently by a linker that wraps around the hinge point, which seems to allow for a much smaller interface in the open conformation. Thus, the buried surface area between monomers is only ~700 Å^2 for pitrilysin.

More detailed comparison between BHP and the eukaryotic M16B enzymes reveals an exception to the rigid body rotation (Figures 5 and S4). Thus, helix α12 packs against the second monomer, making very similar interactions in both the open and closed conformations: in particular, L344 (L386 in MPP) seems to act as a "linchpin," by packing into a pocket at one corner of the N-terminal β sheet of the second monomer. That is, helix α12 remains affixed to the second monomer, and the rotational hinge points leading to clam-shell opening actually occur at either end of this helix. One important prediction of this model is that the environment of α12 changes within its own monomer as a result of clam-shell opening. Of particular note, helix α14 rolls or ratchets around helix α12, burying an exposed hydrophobic surface on α12, as well as forming new contacts with the top edge of the N-terminal β sheet. The burial of hydrophobic surfaces in this local region may compensate, at least in part, for the loss of the more extensive interface in the closed conformation of BHP.

One residue that is solvent-exposed in the closed conformation of BHP, but predicted to become buried in the open conformation, is M343, adjacent to the linchpin residue, L344. We therefore tested our model of the open conformation by making a M343D mutant, predicting that this change would preferentially destabilize the open conformation. The mutant's behavior was indeed consistent with our model: it behaved predominantly as a monomer in solution (Figure S1B), but also retained a surprisingly high level of catalytic activity (see below).

Validation of the "Open" Model Using Small Angle X-ray Scattering (SAXS)

Small-angle X-ray scattering (SAXS) enables the conformations of macromolecules in solution to be analyzed by comparing

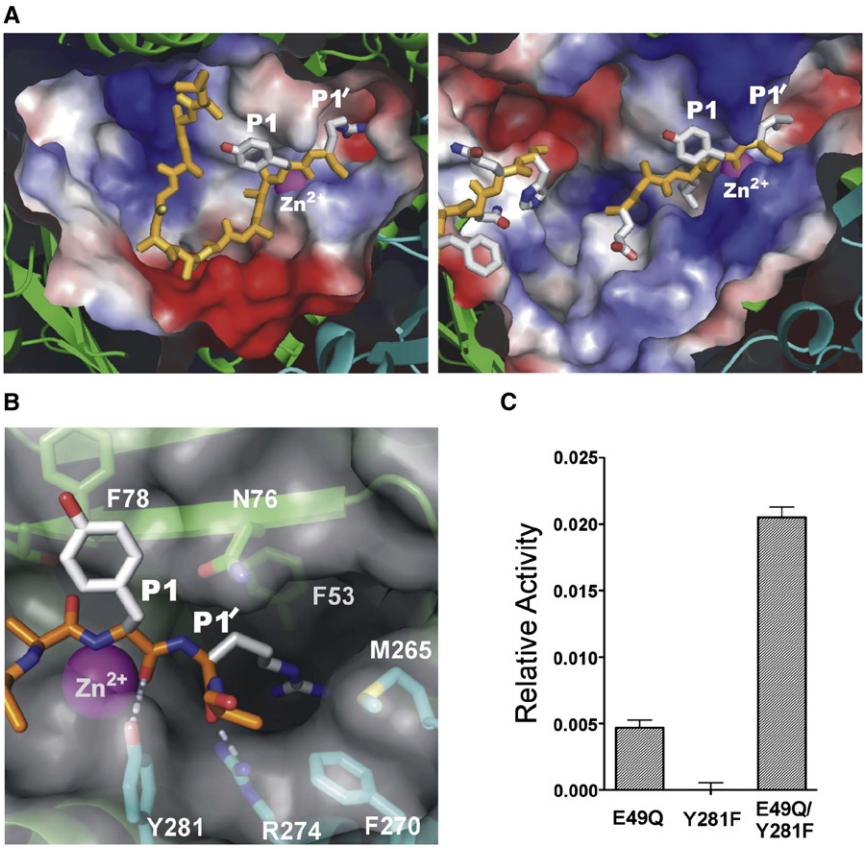

Figure 4. Structure of the Catalytic Chamber, Active Site, and the Role of Domain Closure

(A) Overview of the substrate chambers of BHP (left panel) and IDE (PDB entry 2G48) (right panel) colored by surface charge. The peptide substrates are shown as sticks. The metal ions are indicated.

(B) Hypothetical model of a productive complex. The active site of BHP is shown in green (monomer 1) and blue (monomer 2), covered by a semi-transparent surface. The P1 and P1′ residues are modeled as Tyr (packing against F78) and Arg, which inserts into the hydrophobic/acidic S1' pocket. Selected H-bonds between the peptide and residues from the second monomer are shown.

(C) Relative activities (initial velocities normalized to wild-type) of BHP dimers with point mutations at E49Q or Y281F, or a mixture of the two, showing complementation via heterodimer formation (see main text). The methodology and absolute kinetic parameters are given in Experimental Procedures. Error bars are deviations from mean (n = 2).

experimental scattering curves with those predicted from 3-dimensional atomic models (Putnam et al., 2007), providing a stringent test of our model. We analyzed three samples: wild-type enzyme without substrate; the inactive mutant, E49Q, bound to the insulin-B; and the monomeric M343D mutant described above. Theoretical scattering curves were generated for three models: the crystallographic dimer with insulin-B modeled inside its chamber; the open dimer described above; and a BHP monomer derived from the crystal structure (Figures 6A–C). The theoretical curves have distinctive shapes for each of the 3 models, and the experimental data give an obvious 'best fit' in each case (Figures 6D–6F). Thus, the substrate-bound E49Q mutant conforms best to the closed dimer model; the unligated wild-type enzyme fits the open dimer model; and the M343D mutant conforms to a monomer. A computational analysis using the program OLIGOMER, which optimized the curve-fitting by allowing mixed populations of the three models, gave only marginal improvements in fit for the closed and open dimers, and no improvement for the monomer.

These results are in excellent agreement with the following mechanism of prokaryotic M16B peptidasome action: the molecules adopt a default open dimeric conformation in solution; and the binding of substrate causes the clam-shell to close, bringing the two critical elements of the active sites together. Intriguingly, when tested in the peptide cleavage assay, the M343D mutant showed only a 20-fold reduction in activity. As noted above, this mutation is predicted to destabilize the open conformation (the predominant species in solution in the absence of substrate) but not the closed one. It seems likely that a subset of the mutant protein forms productive dimers, and the gel filtration profile does show a shoulder suggestive of this (Figure S1B). The data can thus be interpreted by assuming a low population of dimers that have high (comparable to wild-type) intrinsic activity, consistent with both predictions of our model.

Implications for the Prokaryotic M16B Family

There are many prokaryotic genes that have been assigned to the M16B subfamily based on sequence alignment (Rawlings et al., 2008). Members of the M16B.016 group (of which BHP is a member) contain the HxxEH and R/Y motifs within a single ~500-residue gene product, and we predict that these will function as homodimeric peptidasomes. However, the M16B.014 and single-domain M16B.UPB groups contain the N-terminal Zn^{2+}-binding motif but lack the C-terminal R/Y pair (Figure 7). We propose that these proteins will form heterodimers with members of the M16B.UNB group, which lack the Zn^{2}-binding motif but contain the R/Y pair, and are typically encoded by adjacent genes. One example is the *B. halodurans* gene-pair, *BH2392* (encodes an M16.014 "peptidase") and *BH2393* (encodes an M16.UNB "nonpeptidase"), which occupy adjacent positions on the genome. A second example is described below.

Thus, the structure of an M16 protein, *T. thermophilus,* TTHA1264, was recently reported (Ohtsuka et al., 2009). This protein is monomeric in solution, and although it crystallized as a homodimer, the authors proposed that the dimer was an artifact of crystallization. Our analysis supports their conclusion: the protein is a member of the M16B.UPB group, and thus lacks the R/Y motif. We therefore predict that TTHA1264 lacks intrinsic protease activity, and that it must form a heterodimer to be functional; the most likely partner is the product of the adjacent gene, TTHA1265, which is a member of the M16B.UNB group (Figure 7).

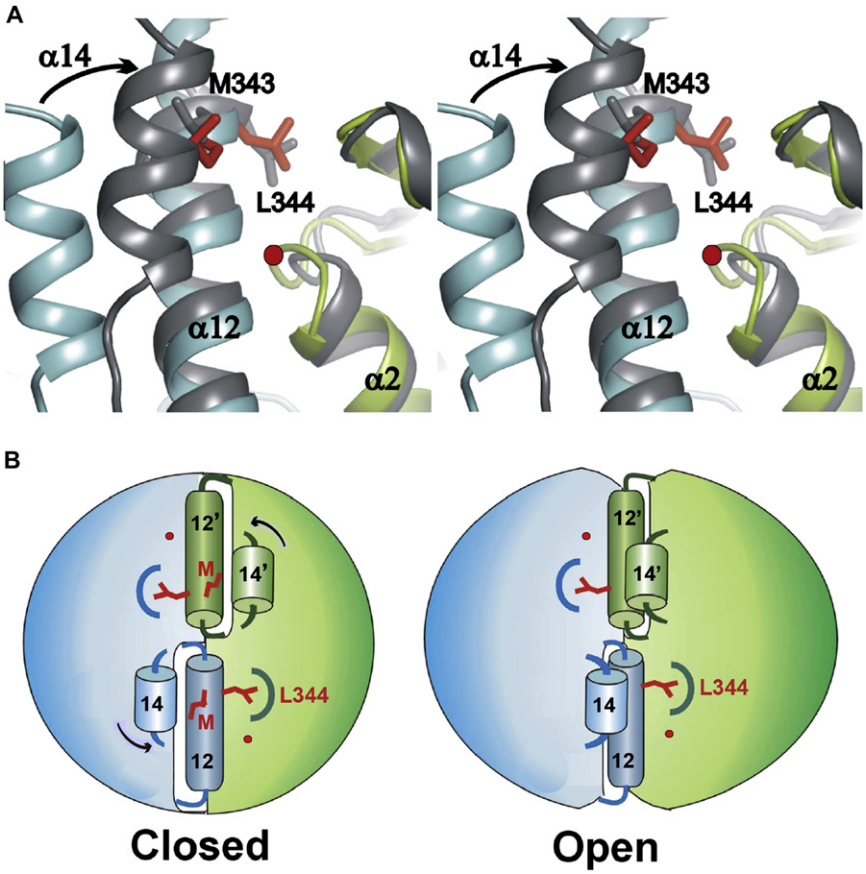

Figure 5. A Hypothetical Model for the Opening of the BHP Clam-shell

(A) Stereo comparison of the structures of BHP (monomers shown in blue and green) and MPP (gray) in the region of the "open" interface of MPP. The α subunit of MPP is overlaid on the green monomer of BHP. The α12 from the blue monomer of BHP packs tightly against the green monomer, as seen from the position of residue L344 and its ortholog in MPP, which insert into the other monomer in a similar fashion, as well as the conserved glycine (red ball) at the tip of helix α2, which allows close packing with α12. α12 does not rotate together with its own monomer. Thus, upon opening of the clam-shell, α14 rolls around α12 (indicated by arrow), burying its hydrophobic surface, including M343.

(B) Cartoon of the proposed clam-shell opening mechanism in the context of the whole BHP dimer, with monomers in blue and green, showing α12 fixed to the other monomer, the rotation of α14 that buries M343 ("M"), the "linchpin" leucine in its pocket, and the conserved glycine (red ball). Symmetry-related helices have primed labels.

Evolution of the M16 Peptidases

The eukaryotic M16B "processing peptidases" that are locked in a partially open conformation lack the R/Y pair (Figure 7). This is expected given that the orthologous residues are held far from the active site. In their place, a long glycine-rich loop emanates from the opposite end of the same helix (α10), reaching down into the active site, where it may play a dual function –contributing residues to the active site and preventing clam-shell closure (Nagao et al., 2000). Interestingly, BHP, as well as other members of the prokaryotic M16B subfamily, contains a shortened version of this loop at the analogous location (Figure 7). In BHP, this loop covers the inward-facing surface of α12 (Figure S4) in both the open and closed conformations, perhaps acting as a flexible "glue" to enhance the stability of this interfacial region. Indeed, portions of the elongated loops in MPP and BC1 appear to play a similar role. By contrast, in the M16A/C peptidasomes, this loop is either absent or has a different environment, consistent with a distinct clam-shell-opening mechanism.

We therefore propose an evolutionary pathway that begins with proteins resembling the BHP/M16B.016 group of homodimeric peptidasomes (Figure 8). In a first step, the loss of one of the Zn-binding motifs leads to the creation of peptidasome with a single active site, similar to M16B.014:M16B.UNB heterodimers. A possible clue as to why such an adaptation would occur comes from the unusual kinetics of peptide hydrolysis by BHP, which exhibit a high level of substrate inhibition, with the K_I value exceeding K_M by only a factor of 4 (see Experimental Procedures; Figure S5); this suggests that the second site acts as an inhibitory site, perhaps via steric interference.

At this point, the pathway diverges, although a heterodimeric organization with a single active site is maintained. One branch leads to the eukaryotic M16B proteases, which have a dimeric organization very similar to the prokaryotic enzymes, but elongation of the glycine-rich loop has inhibited clam-shell closure and created new functionality, as described above. The loss of the R/Y pair is then inevitable because they are no longer required for catalysis.

The second branch leads to the M16A/C peptidasomes, in which the two genes have fused and are connected by a long linker. The presence of a covalent linkage relaxes the structural and mechanistic restraints needed to maintain a stable interface in the open conformation. Thus, in the open structure of pitrilysin, the elaborate hinge mechanism of the dimeric peptidasomes has been dispensed with. The M16A enzyme, pitrilysin, for example, utilizes only one helix and part of the linker region as its hinge (Figures 8, S3). This modification allows a much wider opening of the clamshell than is possible in the dimeric enzymes, such that IDE and pitrilysin can degrade intact insulin, whereas BHP cannot (Cornista et al., 2004; Dabonne et al., 2005).

The open conformation of the M16C peptidasome is currently unknown, but is distinct from the M16A subfamily because the linker is located at the opposite side of the molecules with respect to the active site (Figures 8, S3). It has been suggested that the open conformation of M16C is similar to that of MPP (Johnson et al., 2006), but it seems more likely that the M16C peptidases will operate in a manner similar to that of pitrilysin, but with the hinge located on the opposite side of the molecule (Figure 8).

Summary and Conclusions

The salient conclusions of this study are as follows: (i) BHP functions as a homodimer. (ii) The active site of BHP is similar to those

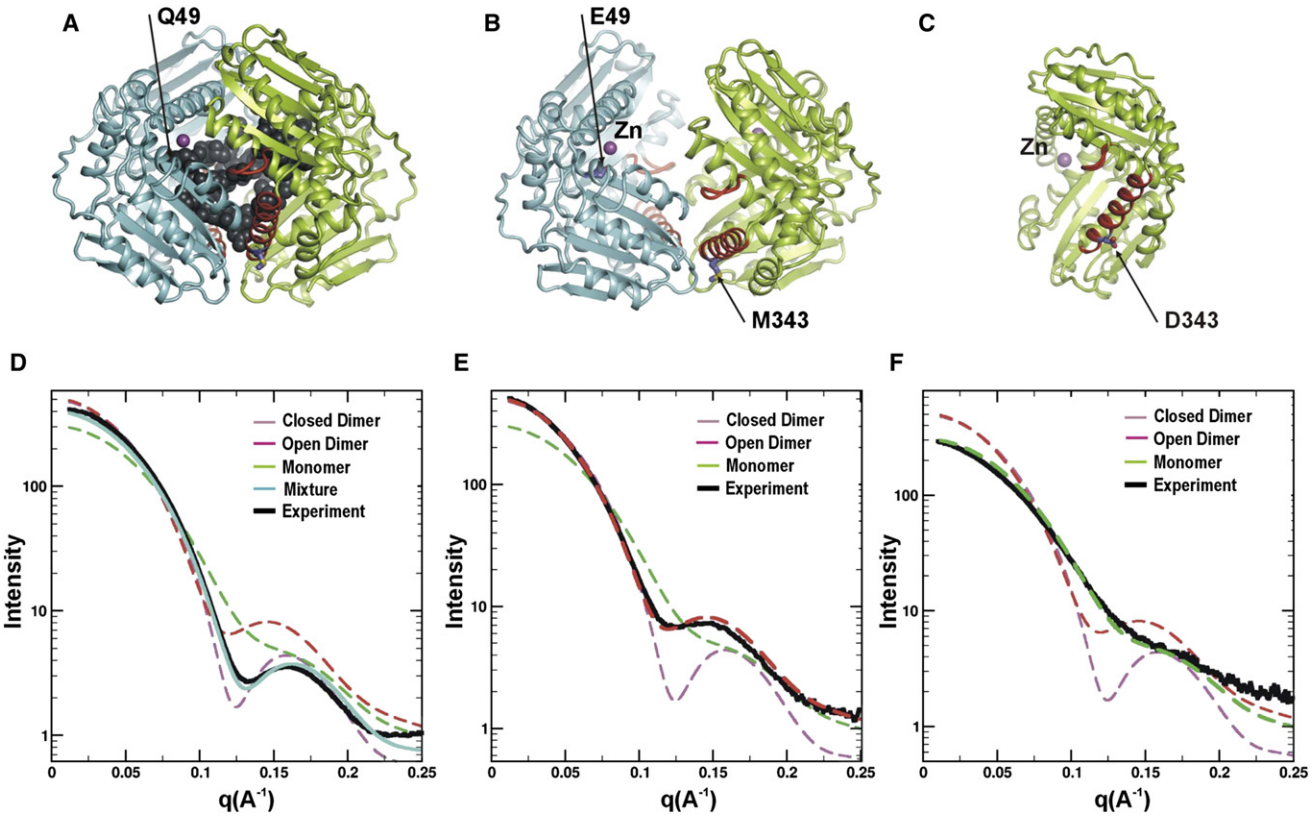

Figure 6. SAXS Analysis of BHP in Solution

(A-C) Model of the closed dimer (A, see main text), the open dimer (B), and monomeric BHP (C).

(D–F) SAXS scattering profiles from: (D) the E49Q inactive mutant in the presence of 250 μM Insulin-B; (E) wild-type BHP in the absence of substrate; and (F) the M343D mutant. Curve-fitting based on the atomic models demonstrates a "best fit" for the closed (D), open (E), and monomeric (F) states.

of the M16A/C peptidasomes, consistent with its peptidasome function, and distinct from M16B eukaryotic processing peptidases. (iii) BHP exists in an open dimeric conformation in the absence of substrate. (iv) The open structure likely resembles the eukaryotic M16B proteins, and closes by means of hinge points at either ends of two fixed helices (α12). (v) Closure of the clam-shell is required for catalytic activity. (vi) We predict the existence of both homodimeric and heterodimeric variants of the prokaryotic M16B peptidasome, with a similar mechanism and function. (vii) The structure and mechanism of BHP suggests that M16B.016 proteins represent the primordial members of the M16 family, suggesting an evolutionary pathway that rationalizes the mechanistic and functional diversification of the entire family.

EXPERIMENTAL PROCEDURES

Cloning, Expression, and Purification of BHP

Genomic DNA from *Bacillus halodurans* C-125 (ATCC) was used for the amplification of the *BH2405* gene. The polymerase chain reaction was carried out with Taq DNA polymerase (Invitrogen) and primers 5′-ATTACGATCCATGGTTAACA-CGATGACGCT-3′ and 5′-ATCGACTTCTCGAGGTGAAT-CAATGCTTTTGGAAG-3′. The gene was cloned in the pET-21d vector and expressed in *E. coli* BL21(DE3)RIL cells. The mutations E49Q and Y281F were obtained using QuikChange Kit (Stratagene) and validated by sequencing. The recombinant protein tagged with a His_6 sequence was purified using nickel-affinity and size-exclusion chromatography. Bacterial cultures were grown at 37°C in LB medium supplemented with ampicillin (100 μg/ml), induced with 0.4 mM IPTG at OD_{600} = 0.5, and grown for an additional 4 hr. Cells from a 5 l culture were collected and lysed by sonication in 50 mM phosphate buffer (pH 8.0), 500 mM NaCl, and 200 μg/ml lysozyme. The supernatant was loaded in the presence of 10 mM imidazole onto a 5 ml HisTrap HP column (GE Healthcare). The column was washed with 10 volumes of 50 mM phosphate buffer (pH 8.0), 500 mM NaCl, and 25 mM imidazole. The protein was eluted in 40 ml 50 mM phosphate buffer (pH 8.0), 500 mM NaCl, and 200 mM imidazole. The resulting samples were purified further by size exclusion chromatography using a Sephacryl S-100 column (GE Healthcare) equilibrated with 30 mM Tris-Cl buffer (pH 8.0) and 100 mM NaCl. The purity of the protein preparation was confirmed by SDS-PAGE (Figure S1A).

Analytical Gel Filtration

Proteins (100 μl at 3–300 μM) were injected into a Superdex200 HR10/30 column (Amersham Biosciences) equilibrated with 100 mM NaCl and 30 mM Tris-Cl (pH 8.0), and eluted at 0.5 ml/min using an ACTA FPLC system. The apparent MW of the sample was calculated from the calibration curve derived from chromatography of MW standards (Bio-Rad).

Kinetic Assay of Peptide Cleavage by BHP

The activity of BHP (at 0.16 μM) was examined at 37°C in 0.1 ml reaction mixtures containing 30 mM Tris/HCl (pH 8.0), 100 mM NaCl, and a fluorescent peptide substrate, Mca-RPPGFSAFK(Dnp)-OH (substrate-V from R&D Systems) (see Figure S5). Initial reaction velocity was monitored continuously at λ_{EX} = 320 nm and λ_{EM} = 405 nm on a Spectramax Gemini EM fluorescence spectrophotometer (Molecular Devices). All assays were performed in duplicate in 96-well plates. The k_{cat}, K_M, and K_I values were derived from the substrate

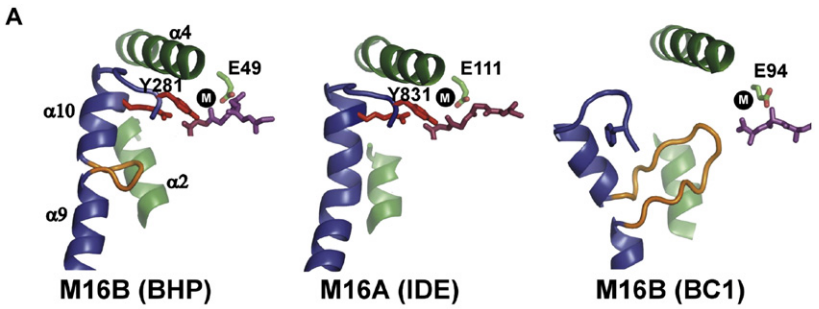

B

GROUP/	GENE	PRODUCT		α1 HHHHH			α9 HHHHHHHH	G-rich loop LLLLLLLLLLLLLLLLL	α10 HHHHHHHHHH	LLLL	
M16A	IDE		108	HFCEH	112	-> 332	HYLGHLIGHEG	----------PGSLLSELKSKGWVNTL			359
			591	NMAYL	595	-> 808	LELFCQII	----------SEPCFNTLRTKEQLGY			831
M16C	PreP		134	HILEH	138	-> 377	GFLDHLCLGTP	----------ASPLRKILLESGLGEAL			404
			652	PLFCQ	656	-> 831	AYVISKHI	----------SNTWLWDRVRVSGGA-Y			911
M16B.016	BHP		46	HFLEH	50	-> 254	LVLLNNVLGGS	----------MSSRLFQDIREKRGLCY			281
M16B.016	BHP		46	HFLEH	50	-> 254	LVLLNNVLGGS	----------MSSRLFQDIREKRGLCY			281
M16B.014	BH2392		67	HFLEH	71	-> 278	INVLLELMFGQ	----------GSKQYEQLDDEGLIND			308
M16B.UNB	BH2393		88	HIITI	92	-> 283	MQVMNGLFGGF	----------SHSKLFINVREKESLAY			310
M16B.UPB	TTHA1264		46	HFLEH	50	-> 255	GQVLAHLLGEE	----------GSGRLHFALVDKGLAEV			282
M16B.UNB	TTHA1265		45	ALLEG	49	-> 251	ARLALEVLSGG	----------MSSRLFTEVREKRGLVY			278
M16B	BC1-I		91	YFVEH	95	-> 289	LQVANAIIGHYDCTYGGGAHLS-	SPLASIAATNKLCQSF			341
M16B	BC1-II		81	HLLRL	85	-> 286	FSVLQHVLGAGPHVKRGSN---	ATSSLYQAVAKGVHQPF			321
M16B	MPP-β		70	HFLEH	74	-> 285	ALATQAIVGNWDRAIGTGTN---	SPSPLAVAASQNGSLA			320
M16B	MPP-α		62	HILDR	66	-> 276	LATLQTLLGGGGSFSAGGPGKGMYS	RLYTHVLNQYYFVE			314

Figure 7. Characteristic Motifs of Peptidasomes and Processing Peptidases

(A) Structural schematics of two peptidasomes (BHP and IDE) and one processing protease (BC1). N-terminal domains are in green, C-terminal domains in blue; glycine-rich loops and R/Y motifs from the α9-α10 region are highlighted in yellow and red; a short substrate segment surrounds the metal ions (black balls). For clarity, only the E of the HxxEH motif is shown.

(B) Sequence fragments of selected functional pairs of N- and C-terminal domains. In all cases (except the homodimeric M16.016 group), the C-terminal domain lacks the Zn-binding motif, but all peptidasomes (M16A/C and prokaryotic M16B subfamilies) contain the R/Y motif in their C-terminal domains, which inserts into the active site as shown in (A). Eukaryotic M16B enzymes (BC1 and MPP) lack the R/Y motif, but contain a large glycine-rich loop (yellow) that plays an analogous role. Peptidasomes (except for the M16A/C C-terminal domains) contain a short loop inserted at the same position, but it is not directly involved in catalysis. Two examples of prokaryotic M16 protein pairs that display the canonical N-terminal (M16B.014 and M16B.UPB) and C-terminal (M16B.UNB) motifs, are encoded by adjacent genes, and are predicted to form functional heterodimers, are shown: BH2392/BH2393 from *B. halodurans* and TTHA1264/1265 from *Thermus thermophilus*.

inhibition equation provided in Prism-5: $V = k_{cat}[BHK][S]/((K_M+[S])(1+[S]/K_I))$. The following kinetic parameters were obtained: $k_{cat} = 0.16 \pm 0.03\ s^{-1}$, $K_M = 5.0 \pm 1.4\ \mu M$, $k_{cat}/K_M = 32{,}000\ M^{-1}\ sec^{-1}$, $K_I = 20.6 \pm 6.4\ \mu M$. For the comparison of activities of the mutants (Y281F, E49Q, and M343D), initial velocities using 0.1–0.5 μM BHP with 10 μM substrate-V were measured (see Figure 4C). The absolute values of the initial velocities scaled to 1 μM enzyme were $69 \pm 4 \times 10^{-3}$ μM/s (WT); $0.34 \pm 0.03 \times 10^{-3}$ μM/s (E49Q); $0.000 \pm 0.003 \times 10^{-3}$ μM/s (Y281F), and $3.7 \pm 0.1 \times 10^{-3}$ μM/s (M343D).

Small Angle X-ray Scattering

SAXS data were collected from the wild-type BHP in the absence of substrate, and from two mutants. Proteins were prepared in 150 mM NaCl, 30 mM Tris-Cl buffer (pH 8.0), and concentrations varied from 1 to 3 mg/ml (~25–75 μM). The inactive E49Q mutant was incubated with 250 μM Insulin-B (Sigma). An M343D mutant, which is monomeric by gel filtration, was used as a control. SAXS data were collected at the SIBYLS beamline (BL1231) at the Advanced Light Source at the Lawrence Berkeley National Laboratory. Data were collected using 12 keV X-rays with a sample-to-detector distance of 1.5 m. Samples volumes of 12 μl were loaded using a pipetting robot as previously described (Hura et al., 2009). No correction was required for concentration dependence for the profiles shown. Buffer controls were collected before and after data collection to provide an accurate solvent correction. X-ray exposures of 0.5 and 5 s were collected and merged. The programs CRYSOL and OLIGOMER (Konarev et al., 2003) were used to calculate scattering profiles based on atomic coordinates, and to estimate the population of each conformational state in solution.

Crystallization and X-ray Data Collection

BHP was crystallized by the hanging drop vapor diffusion method. 1.5 μl of 10–20 mg/ml (0.2-0.4 mM) protein in 25 mM HEPES, 50 mM NaCl (pH 7.5) was mixed with 1.5 μl crystallization buffer containing 1–10 mM $CoCl_2$, 0.1 M MES at pH 6.5, and 1.8 M $(NH_4)_2SO_4$. We observed that the sample contained a significant amount of a peptide with a MW of ~6 kDa that copurified with BHP by gel-filtration chromatography (Figure S1A). Crystals grew as trapezoidal prisms in space group $C222_1$, typically appeared after several weeks, and grew slowly for an additional 1–3 months to reach 40 × 100 × 200 μm^3 in size. Crystals were transferred to a Co^{2+}-free crystallization buffer containing 30% w/v glucose for 20 min, and then flash-frozen in liquid nitrogen. Prior to data collection, EXAFS spectra were collected at the Co^{2+} and Zn^{2+} absorption edges using beamline 9-1. The spectra indicated the presence of Co^{2+} and the absence of Zn^{2+}. Diffraction data were collected to 2.75 Å resolution on beamline 11-1 at the Stanford Synchrotron Radiation Laboratory. Data were processed using HKL2000 (Minor et al., 2006), and the structure was solved by molecular replacement (PHASER [McCoy, 2007]) using the β-subunit of MPP (sequence identity 29%, PDB entry 2FGE) as the search probe. The model was built using COOT (Emsley and Cowtan, 2004) and XtalView (McRee, 1999), and refined using CNS (Brunger et al., 1998) to $R_{work} = 0.197$ and $R_{free} = 0.269$. The final model contains a dimer of BHP in the asymmetric unit, 2 Co^{2+} ions bound at 100% occupancy (as judged by their B values), two alternate conformers of a peptide (17 residue), which had regions of poor connectivity, each assigned with 50% occupancy, and several sulfate anions. The entire protein had clearly interpretable electron density, with the exception of the N-terminal methionines and His-tags. Data collection and refinement statistics are shown in Table 1.

Structural Comparisons

The structure of BHP and bound peptide ligand were compared with IDE bound to amylin (PDB entry 2G48); the processing peptidase from BC1 complex (1BE3); MPP bound to a signal peptide (1HR9); PreP bound to an unknown peptide (2FGE); pitrilysin (1Q2L); and the *Thermus thermophilus* gene product, TTHA1264 (1EOQ). The structures were aligned by Swiss-PdbViewer (Guex and Peitsch, 1997). Protein sequences were aligned with STRAP (Gille and Frommel, 2001). Structural figures were prepared using PYMOL (DeLano, 2002).

ACCESSION NUMBERS

The atomic coordinates and structure factors have been deposited in the Protein Data Bank with ID code 3HDI.

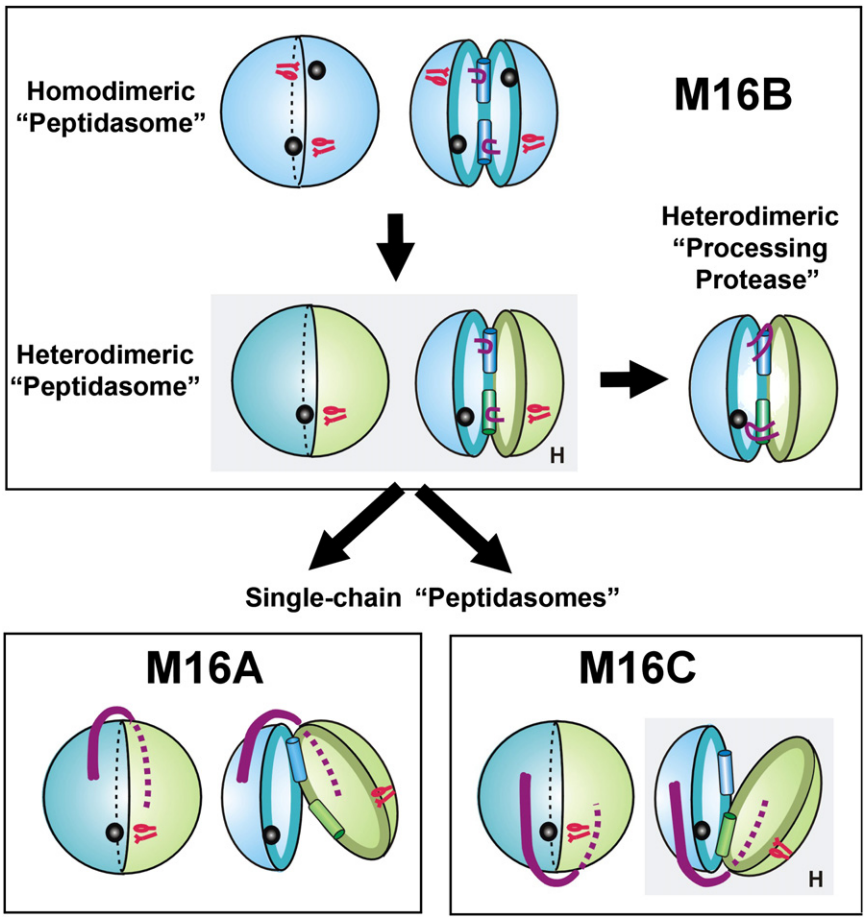

Figure 8. A Model for the Evolution of M16 Peptidases

Closed and open clam-shells are shown for each evolutionary step, indicated by arrows, with a branch point at the heterodimeric processing peptidasomes. Zinc ions are shown as black balls; the R/Y pair as red sticks; the glycine-rich loops as red hoops. Zn^{2+} binding subunits/domains are in blue; the α12 helix pair are shown as cylinders; the interdomain linkers in the M16A/C peptidasomes as red ribbons. Structures lacking experimental verification are labeled "H"; these are the prokaryotic heterodimers, modeled on BHP; and the open conformation of M16C, modeled by analogy with pitrilysin of M16A. As noted in the text, a fraction of the M16B.UPB genes contain the "catalytic" and "noncatalytic" domains fused together, and may represent a transitional group between the M16B and M16A/C architectures; they have been omitted here for simplicity.

SUPPLEMENTAL DATA

Supplemental Data include five figures and can be found with this article online at http://www.cell.com/structure/supplemental/S0969-2126(09)00377-3.

ACKNOWLEDGMENTS

This work was supported by grant NIH AI061139 (to A.Y.S., J.W.S., and R.C.L.). We would like to thank Sheryl Harvey for her assistance with the purification of *B. halodurans* peptidase and Laurie Bankston for helpful discussions. We are also grateful to the staff at the Stanford Synchrotron Radiation Laboratory and the Advanced Light Source at the Lawrence Berkeley National Laboratory (national facilities supported by the NIH and DOE) for beamline maintenance and assistance during data collection.

Received: May 15, 2009
Revised: August 22, 2009
Accepted: September 4, 2009
Published: November 10, 2009

REFERENCES

Becker, A.B., and Roth, R.A. (1992). An unusual active site identified in a family of zinc metalloendopeptidases. Proc. Natl. Acad. Sci. USA *89*, 3835–3839.

Bhushan, S., Lefebvre, B., Stahl, A., Wright, S.J., Bruce, B.D., Boutry, M., and Glaser, E. (2003). Dual targeting and function of a protease in mitochondria and chloroplasts. EMBO Rep. *4*, 1073–1078.

Bolhuis, A., Koetje, E., Dubois, J.Y., Vehmaanpera, J., Venema, G., Bron, S., and van Dijl, J.M. (2000). Did the mitochondrial processing peptidase evolve from a eubacterial regulator of gene expression? Mol. Biol. Evol. *17*, 198–201.

Brunger, A.T., Adams, P.D., Clore, G.M., DeLano, W.L., Gros, P., Grosse-Kunstleve, R.W., Jiang, J.S., Kuszewski, J., Nilges, M., Pannu, N.S., et al. (1998). Crystallography & NMR system: A new software suite for macromolecular structure determination. Acta Crystallogr. D Biol. Crystallogr. *54*, 905–921.

Cabrol, C., Huzarska, M.A., Dinolfo, C., Rodriguez, M.C., Reinstatler, L., Ni, J., Yeh, L.A., Cuny, G.D., Stein, R.L., Selkoe, D.J., and Leissring, M.A. (2009). Small-molecule activators of insulin-degrading enzyme discovered through high-throughput compound screening. PLoS ONE *4*, e5274.

Cornista, J., Ikeuchi, S., Haruki, M., Kohara, A., Takano, K., Morikawa, M., and Kanaya, S. (2004). Cleavage of various peptides with pitrilysin from Escherichia coli: kinetic analyses using beta-endorphin and its derivatives. Biosci. Biotechnol. Biochem. *68*, 2128–2137.

Dabonne, S., Moallic, C., Sine, J.P., Niamke, S., Dion, M., and Colas, B. (2005). Cloning, expression and characterization of a 46.5-kDa metallopeptidase from Bacillus halodurans H4 sharing properties with the pitrilysin family. Biochim. Biophys. Acta *1725*, 136–143.

DeLano, W.L. (2002). The PyMOL Molecular Graphics System (Palo Alto, CA, USA: DeLano Scientific).

Deng, K., Shenoy, S.K., Tso, S.C., Yu, L., and Yu, C.A. (2001). Reconstitution of mitochondrial processing peptidase from the core proteins (subunits I and II) of bovine heart mitochondrial cytochrome bc(1) complex. J. Biol. Chem. *276*, 6499–6505.

Eggleson, K.K., Duffin, K.L., and Goldberg, D.E. (1999). Identification and characterization of falcilysin, a metallopeptidase involved in hemoglobin

catabolism within the malaria parasite Plasmodium falciparum. J. Biol. Chem. *274*, 32411–32417.

Emsley, P., and Cowtan, K. (2004). Coot: model-building tools for molecular graphics. Acta Crystallogr. D Biol. Crystallogr. *60*, 2126–2132.

Farris, W., Mansourian, S., Chang, Y., Lindsley, L., Eckman, E.A., Frosch, M.P., Eckman, C.B., Tanzi, R.E., Selkoe, D.J., and Guenette, S. (2003). Insulin-degrading enzyme regulates the levels of insulin, amyloid beta-protein, and the beta-amyloid precursor protein intracellular domain in vivo. Proc. Natl. Acad. Sci. USA *100*, 4162–4167.

Gille, C., and Frommel, C. (2001). STRAP: editor for STRuctural Alignments of Proteins. Bioinformatics *17*, 377–378.

Guex, N., and Peitsch, M.C. (1997). SWISS-MODEL and the Swiss-PdbViewer: an environment for comparative protein modeling. Electrophoresis *18*, 2714–2723.

Hedengren-Olcott, M., Byrd, C.M., Watson, J., and Hruby, D.E. (2004). The vaccinia virus G1L putative metalloproteinase is essential for viral replication in vivo. J. Virol. *78*, 9947–9953.

Hura, G.L., Menon, A.L., Hammel, M., Rambo, R.P., Poole, F.L., 2nd, Tsutakawa, S.E., Jenney, F.E., Jr., Classen, S., Frankel, K.A., Hopkins, R.C., et al. (2009). Robust, high-throughput solution structural analyses by small angle X-ray scattering (SAXS). Nat. Methods *6*, 606–612.

Im, H., Manolopoulou, M., Malito, E., Shen, Y., Zhao, J., Neant-Fery, M., Sun, C.Y., Meredith, S.C., Sisodia, S.S., Leissring, M.A., and Tang, W.J. (2007). Structure of substrate-free human insulin-degrading enzyme (IDE) and biophysical analysis of ATP-induced conformational switch of IDE. J. Biol. Chem. *282*, 25453–25463.

Johnson, K.A., Bhushan, S., Stahl, A., Hallberg, B.M., Frohn, A., Glaser, E., and Eneqvist, T. (2006). The closed structure of presequence protease PreP forms a unique 10,000 Angstroms3 chamber for proteolysis. EMBO J. *25*, 1977–1986.

Kitada, S., Uchiyama, T., Funatsu, T., Kitada, Y., Ogishima, T., and Ito, A. (2007). A protein from a parasitic microorganism, Rickettsia prowazekii, can cleave the signal sequences of proteins targeting mitochondria. J. Bacteriol. *189*, 844–850.

Konarev, P.V., Volkov, V.V., Sokolova, A.V., Koch, M.H.J., and Svergun, D.I. (2003). PRIMUS: a Windows PC-based system for small-angle scattering data analysis. J. Appl. Crystallogr. *36*, 1277–1282.

Kurochkin, I.V. (2001). Insulin-degrading enzyme: embarking on amyloid destruction. Trends Biochem. Sci. *26*, 421–425.

Kwak, S.H., Cho, Y.M., Moon, M.K., Kim, J.H., Park, B.L., Cheong, H.S., Shin, H.D., Jang, H.C., Kim, S.Y., Lee, H.K., and Park, K.S. (2008). Association of polymorphisms in the insulin-degrading enzyme gene with type 2 diabetes in the Korean population. Diabetes Res. Clin. Pract. *79*, 284–290.

Li, P., Kuo, W.L., Yousef, M., Rosner, M.R., and Tang, W.J. (2006). The C-terminal domain of human insulin degrading enzyme is required for dimerization and substrate recognition. Biochem. Biophys. Res. Commun. *343*, 1032–1037.

Makarova, K.S., and Grishin, N.V. (1999). Thermolysin and mitochondrial processing peptidase: how far structure-functional convergence goes. Protein Sci. *8*, 2537–2540.

Malito, E., Hulse, R.E., and Tang, W.J. (2008). Amyloid beta-degrading cryptidases: insulin degrading enzyme, presequence peptidase, and neprilysin. Cell. Mol. Life Sci. *65*, 2574–2585.

McCoy, A.J. (2007). Solving structures of protein complexes by molecular replacement with Phaser. Acta Crystallogr. D Biol. Crystallogr. *63*, 32–41.

McRee, D.E. (1999). XtalView/Xfit–A versatile program for manipulating atomic coordinates and electron density. J. Struct. Biol. *125*, 156–165.

Minor, W., Cymborowski, M., Otwinowski, Z., and Chruszcz, M. (2006). HKL-3000: the integration of data reduction and structure solution–from diffraction images to an initial model in minutes. Acta Crystallogr. D Biol. Crystallogr. *62*, 859–866.

Nagao, Y., Kitada, S., Kojima, K., Toh, H., Kuhara, S., Ogishima, T., and Ito, A. (2000). Glycine-rich region of mitochondrial processing peptidase alpha-subunit is essential for binding and cleavage of the precursor proteins. J. Biol. Chem. *275*, 34552–34556.

Ohtsuka, J., Ichihara, Y., Ebihara, A., Nagata, K., and Tanokura, M. (2009). Crystal structure of TTHA1264, a putative M16-family zinc peptidase from Thermus thermophilus HB8 that is homologous to the beta subunit of mitochondrial processing peptidase. Proteins *75*, 774–780.

Putnam, C.D., Hammel, M., Hura, G.L., and Tainer, J.A. (2007). X-ray solution scattering (SAXS) combined with crystallography and computation: defining accurate macromolecular structures, conformations and assemblies in solution. Q. Rev. Biophys. *40*, 191–285.

Rawlings, N.D., and Barrett, A.J. (1991). Homologues of insulinase, a new superfamily of metalloendopeptidases. Biochem. J. *275*, 389–391.

Rawlings, N.D., Morton, F.R., Kok, C.Y., Kong, J., and Barrett, A.J. (2008). MEROPS: the peptidase database. Nucleic Acids Res. *36*, D320–D325.

Selkoe, D.J. (2001). Clearing the brain's amyloid cobwebs. Neuron *32*, 177–180.

Shen, Y., Joachimiak, A., Rosner, M.R., and Tang, W.J. (2006). Structures of human insulin-degrading enzyme reveal a new substrate recognition mechanism. Nature *443*, 870–874.

Sun, M.K., and Alkon, D.L. (2006). Links between Alzheimer's disease and diabetes. Timely Top. Med. Cardiovasc. Dis. *10*, E24.

Taylor, A.B., Smith, B.S., Kitada, S., Kojima, K., Miyaura, H., Otwinowski, Z., Ito, A., and Deisenhofer, J. (2001). Crystal structures of mitochondrial processing peptidase reveal the mode for specific cleavage of import signal sequences. Structure *9*, 615–625.

Xia, D., Yu, C.A., Kim, H., Xia, J.Z., Kachurin, A.M., Zhang, L., Yu, L., and Deisenhofer, J. (1997). Crystal structure of the cytochrome bc1 complex from bovine heart mitochondria. Science *277*, 60–66.